

A new classification of ex-situ and in-situ Galactic globular clusters based on a method trained on Milky Way analogues in the TNG50 cosmological simulations

Pierre Boldrini¹, Paola Di Matteo¹, Chervin Laporte^{1,4,5}, Oscar Agertz², Sergey Khoperskov³ and Giulia Pagnini⁶

¹ LIRA, Observatoire de Paris, Université PSL, Sorbonne Université, Université Paris Cité, CY Cergy Paris Université, CNRS, 92190 Meudon, France,

² Lund Observatory, Division of Astrophysics, Department of Physics, Lund University, Box 43, SE-221 00 Lund, Sweden,

³ Leibniz-Institut für Astrophysik Potsdam (AIP), An der Sternwarte 16, 14482 Potsdam, Germany,

⁴ Kavli IPMU (WPI), UTIAS, The University of Tokyo, Kashiwa, Chiba 277-8583, Japan,

⁵ Institut de Ciències del Cosmos (ICCUB), Universitat de Barcelona, Martí i Franquès 1, E-08028 Barcelona, Spain,

⁶ Université de Strasbourg, CNRS, Observatoire astronomique de Strasbourg, UMR 7550, F-67000 Strasbourg, France

submitted to A&A

ABSTRACT

We present a novel method combining existing cosmological simulations and orbital integration to study the hierarchical assembly of globular cluster (GC) populations in the Milky Way (MW). Our method models the growth and evolution of GC populations across various galactic environments as well as the dynamical friction and mass-loss experienced by these objects. This allows us to follow track the trajectory of $\sim 18,000$ GCs over cosmic time in 198 MW-like galaxies from TNG50. This cosmological-scale tracking of the dynamics of in-situ and ex-situ GC populations with such a large statistical sample allows us to confirm the presence of an overlap between the two populations in MW-like galaxies, occurring below an energy threshold of $E < 0.7E_{\text{circ}}(r_{\text{hm}}^*)$ where $E_{\text{circ}}(r_{\text{hm}}^*)$ is the energy of a circular orbit at the galaxy's stellar half-mass radius r_{hm}^* . Our results challenge the validity of current classification schemes commonly adopted in the literature, which ultimately fail to provide a clear separation between the two populations. Instead, they tend to isolate only a subset of the ex-situ GCs. More precisely, we argue that it is highly unlikely to find in-situ clusters at $E > 0.7E_{\text{circ}}(r_{\text{hm}}^*)$, and that the real challenge lies in distinguishing the two populations below this energy threshold. In this context, we provide new predictions regarding the origins of the MW's GCs observed with Gaia, as well as a comparison with existing literature. Additionally, we highlight that even if ex-situ clusters share a common origin, they inevitably lose their dynamical coherence in the E - L_z space within MW-like galaxies. We observe a dispersion of GC groups as a function of E and L_z , primarily driven by the evolution of the galactic potential over time and by dynamical friction, respectively.

Key words. galaxy dynamics - globular clusters - Milky Way - methods: orbital integrations - cosmological simulations

1. Introduction

The study of the Milky Way (MW) provides a unique perspective on galaxy assembly history, serving as a crucial benchmark for theories of galaxy formation and evolution. Among the various stellar systems within the MW, globular clusters (GCs) play a fundamental role as ancient relics that encode essential information about the galaxy's assembly history. A key aspect of MW GCs is their diverse origins: while some are thought to have formed in-situ within the progenitor of the MW, others were accreted (ex-situ) through the mergers of satellite galaxies (Forbes & Bridges 2010; Massari et al. 2019; Kruijssen et al. 2019b; Helmi 2020; van den Bergh 2012; Leaman et al. 2013; Mackey & van den Bergh 2005). Studies of GCs in external galaxies, such as the analysis of accreted GCs in M31 by Andersson & Davies (2019), provide complementary insights into the processes of GC accretion and the signatures of past merger events.

Identifying and characterizing these two populations is essential for reconstructing the accretion history and evolutionary pathway of our Galaxy. This has become possible thanks to

the full six-dimensional phase-space information available for nearly all Galactic GCs from the third data release of the Gaia mission (Gaia Collaboration et al. 2018, 2021), which has provided unprecedented insights into their dynamics (Vasiliev & Baumgardt 2021). In principle, these data contain fundamental information about the origin of the clusters themselves – that is whether a given GC formed within the MW or originated in a satellite galaxy that was later accreted. However, the question that the community is currently facing is how to analyse and interpret these data in order to discern the origin of Galactic GCs. Various methods (see, for example, Massari et al. 2019; Forbes & Bridges 2010; Kruijssen et al. 2020, 2019a; Malhan et al. 2022; Myeong et al. 2018) have been developed to classify GCs as in-situ or ex-situ, leveraging their kinematic, spatial, age and chemical abundance properties with the latter being provided in part by spectroscopic surveys (e.g. APOGEE Majewski et al. 2017). In particular, the distribution of GCs in integral-of-motion spaces, such as the energy-angular momentum E – L_z plane, is inhomogeneous. This inhomogeneity suggests the presence of groups of GCs with distinct spatial and kinematic properties. Clusters located close to each other in this integral-of-motion space are thought to share a common ori-

Send offprint requests to: Pierre Boldrini, e-mail: pierre.boldrini@obspm.fr

gin, potentially reflecting different formation histories, either in-situ or through accretion (Chen & Gnedin 2024; Belokurov & Kravtsov 2023; Massari et al. 2019; Malhan et al. 2022; Pfeffer et al. 2020; Sun et al. 2023). More recently, novel approaches which have complemented analysis in the $E-L_z$ plane with mean chemical abundance ratios such as $[Al/Fe]$ have been also introduced to refine the quest of accreted and in-situ GCs (Belokurov & Kravtsov 2024).

However, Pagnini et al. (2023) challenged the idea of a dynamical coherence among accreted GCs, emphasizing that even the debris from a single merger event can span a wide range in the $E-L_z$ space, as well as in all kinematic spaces used so far, including actions space. They argue that the assumption that accreted clusters should exhibit a clear dynamical coherence, that is a tendency to cluster in kinematic spaces, remains unproven, and in general is not physically motivated. Moreover, E and L_z are not conserved quantities in a time-evolving non-axisymmetric galaxy (Binney & Tremaine 2008), due to the significant growth of the galaxy's mass over time and the mergers of massive satellites, which perturb both the accreted and in-situ components of the galaxy. As a result, relying solely on the present-day ($z = 0$) distribution in the $E-L_z$ space to infer the origin of GCs can be misleading, requiring additional information and potentially the study of their temporal evolution. The results in (Pagnini et al. 2023) are consistent with findings for field stars, for which it is also challenging to uncover their nature using kinematic spaces (Jean-Baptiste et al. 2017; Amarante et al. 2022), even when supplemented with abundance information (Khoperskov et al. 2023a,b; Mori et al. 2024). The difficulty encountered in establishing the origin of the stars and GCs in our Galaxy by making use of energy and angular momentum (eventually supplemented by other properties) is illustrated for example by the case of Omega Centauri (NGC 5139), which is likely the former nuclear star cluster of an accreted galaxy, as suggested - among other unusual properties - by its broad metallicity spread (Lee et al. 1999; Majewski et al. 2000; Carraro & Lia 2000; Bekki & Freeman 2003; Tsuchiya et al. 2004, 2003). While some classifications might place it among in-situ GCs (Belokurov & Kravtsov 2024; Chen & Gnedin 2024), others support an ex-situ origin for this system (Massari et al. 2019; Forbes & Bridges 2010; Pfeffer et al. 2021).

Studying the dynamics of GCs over cosmological timescales and within cosmological environments is crucial for understanding the formation and evolutionary history of galaxies like the MW. However, due to the vast spatial and temporal scales involved, simulating these objects presents significant challenges, leading to the adoption of various approaches, each with their inherent limitations (for reviews, see Beasley (2020); Renaud (2020a)). Three main strategies have emerged for modeling GC dynamics, incorporating increasingly sophisticated models of GC formation. A common approach relies on idealized galaxy simulations with pc resolution, which enables the study of clustered star formation at high redshift. However, most of these simulations do not robustly reproduce GCs in terms of their sizes, masses, or chemical properties (Lahén et al. 2020; Li et al. 2022; Deng et al. 2024; Andersson et al. 2024). Besides, these simulations can only model faint galaxies and in small numbers (typically one or two) and are limited in their evolutionary timescale (typically up to 1 Gyr) due to their high computational cost. Another strategy involves high-resolution cosmological zoom-in simulations, which enhance spatial resolution and allow for the study of GC formation in a more realistic cosmological setting (Kravtsov & Gnedin 2005; Li et al. 2017; Kim et al. 2018; Ma et al. 2020; Meng & Gnedin 2022;

Sameie et al. 2023; Dubois et al. 2021). While these simulations achieve extremely high mass resolution (resolving dwarf galaxies) and spatial resolution (down to 10 pc), they are typically restricted to high redshifts ($z = 3-5$). To overcome these spatial and temporal limitations, one approach involves incorporating semi-analytical models within hydrodynamical simulations to form and track the evolution of GCs (Pfeffer et al. 2018; Reina-Campos et al. 2022; Grudić et al. 2023; Newton et al. 2024; Rodriguez et al. 2023). However, this does not reduce the computational cost of hydrodynamical simulations, which remain limited to a small number of galaxies (typically 1–21 MW-like galaxies). To achieve larger statistical samples, an alternative approach is to apply "tagging" techniques in post-processing (Bullock & Johnston 2005; Cooper et al. 2010; Laporte et al. 2013; Renaud et al. 2017a; Ramos-Almendares et al. 2020; Halbesma et al. 2020; Park et al. 2022; Doppel et al. 2023; Chen & Gnedin 2023; Creasey et al. 2019). In these methods, GCs are "painted" onto simulation particles (either dark matter (DM) or stars) following specific prescriptions. These techniques are computationally inexpensive, as they do not require rerunning simulations to modify the GC formation and evolution model parameters, and they enable the study of a large number of galaxies (up to $N = 8000$) in diverse environments. Although various tagging techniques exist to study GCs, either by tagging GCs at multiple epochs to analyze their properties within galaxies, or by inferring their dynamics from star or DM particles within simulations, no study has applied these methods on a large statistical sample of Milky Way-like galaxies in a self-consistent manner. Our approach stands out by applying it to nearly 200 Milky Way-like galaxies from TNG50, enabling a statistically robust analysis of GC dynamics from formation to $z = 0$. Therefore, developing a complete picture of GC dynamics requires combining tagging techniques in cosmological hydrodynamical simulations with orbit integration methods. In principle, coupling these approaches could allow for the self-consistent tracking of GC dynamics within a cosmological environment over a Hubble time.

In this paper, we revisit the challenge of distinguishing between in-situ and ex-situ GC populations in MW-like galaxies, focusing on their identification within the $E-L_z$ space. Our analysis is conducted in a full cosmological context, including satellite galaxy accretions and a time-evolving potential for the host galaxy, both of which affect GC dynamics. To achieve this, we follow the spatial evolution of a population of tens of thousands of GCs within a cosmological framework, leveraging orbital integration techniques in combination with the TNG50 simulation. The paper is structured as follows: Section 2 outlines our methodology, which describes our post-processing orbital integration method for globular clusters in cosmological simulations. In Section 3, we present and discuss our results, comparing them with Gaia data for the MW's GC system. Finally, Section 4 provides our conclusions.

2. Methods: combining orbital integration methods in post-processing with TNG50 simulation

To track the dynamics of GCs over cosmological timescales in a galaxy like the MW, it is essential to consider its merger history, which plays a key role in constructing the observed GC population at $z = 0$. By providing access to the evolutionary history of 198 MW analogues, the hydrodynamical cosmological simulation TNG50 (Nelson et al. 2019b,a; Pillepich et al. 2019) enables us to reconstruct the time-evolving gravitational potentials that account for both the evolution of the MW and

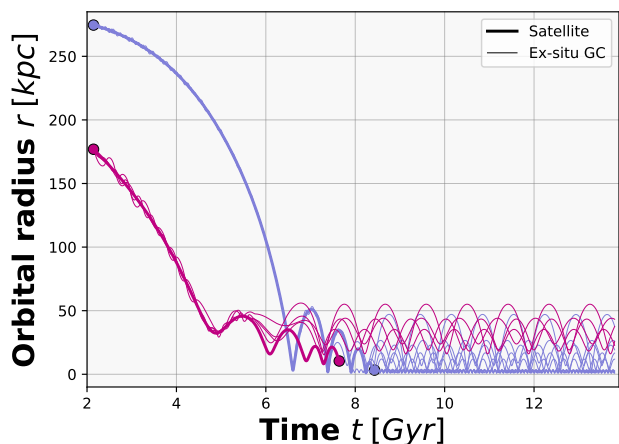


Fig. 1. Orbital radius as function of time for two merging galaxies (IDs 383325 and 299509) with their associated GCs. The points mark the formation and merger times of the satellites from TNG50. During the initial phase, ex-situ GCs orbit within the reference frame of their satellite galaxy until their orbital energy becomes positive ($E > 0$). Once this condition is met, GCs are transferred to the MW’s reference frame while maintaining the moving potential of the satellite galaxy if it has not yet merged.

its environment through satellite galaxy accretion. TNG50¹ is a high-resolution cosmological hydrodynamical simulation with a 51.7 Mpc box and 2160³ particles, reaching a baryonic mass resolution of $8.4 \times 10^4 M_\odot$ and $4.5 \times 10^5 M_\odot$ for dark matter. With a gravitational softening of 288 pc at $z=0$, it includes detailed models for star formation, chemical enrichment, black hole growth, AGN feedback, and galactic winds (Weinberger et al. 2017; Pillepich et al. 2018). Besides, Pillepich et al. (2024) provide masses and half-mass radii at different redshifts of these MW-analogues and their associated satellites. By assigning a GC population to each MW progenitor and its satellite population at high- z , we can follow their dynamical evolution through orbital integration using the publicly available code galpy² (Bovy 2015), taking into account both dynamical friction and mass loss for these time evolving MW-like potentials from $z = 3$ to the present-day. In the following, we first describe the MW-like potentials, then how we defined initial conditions for our GCs systems at high- z , and finally how we performed the orbit integration.

2.1. TNG50 Milky Way-like potentials

The 198 MW analogues identified in the TNG50 simulation have global properties, such as stellar mass between $10^{10.5} M_\odot$ and $10^{11.2} M_\odot$ and large-scale environment, that is similar to those of our Galaxy. Up to 7 Gyr backwards in time, the mean stellar mass of the TNG50 MW analogues is in good agreement with the mass evolution of our Galaxy derived by Snaith et al. (2015) (see Figure 2). We extract the structural parameters (masses and half-mass radii) of the MWs and their associated merging satellites across 75 snapshots from $z = 3$ to 0. Actually for TNG50, snapshots at all 100 available redshifts, galaxy catalogs at each snapshot and merger trees are released. We focus on identifying all the satellites that merged with our MW-like galaxies during

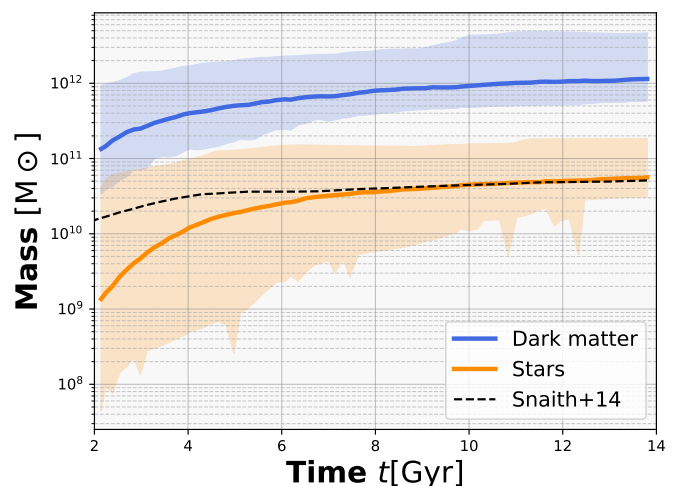


Fig. 2. The mass evolution of the stellar and DM components of the MW for our full sample of 198 MW analogues from TNG50 is shown. Up to 7 Gyr backwards in time, the mean stellar mass of the TNG50 MW analogues is in good agreement with the mass evolution of our Galaxy derived by Snaith et al. (2015).

this period, retaining only those with a stellar mass greater than $10^7 M_\odot$, in line with the TNG50 mass resolution ($4.5 \times 10^5 M_\odot$ for DM particles and $8.5 \times 10^4 M_\odot$ for the stellar component). We modeled the potentials of the MW-like galaxies by using a Hernquist (1990) profile for stars and an NFW profile for DM (Navarro et al. 1997), with the parameters computed based on the properties found in TNG50. These MW-like potentials evolve over time, and the evolution of the masses and scale radii is incorporated into our model. Specifically, we update the potential 75 times during the orbit integrations. Satellite galaxies are also modeled with two potential components: a Hernquist (1990) profile for stars and a NFW DM halo (Navarro et al. 1997).

To summarize, from the masses and half-mass radii provided by TNG50, we can derive 198×75 MW-analogues composite stellar+DM gravitational potentials. Each of these MW analogues is surrounded by its processions of satellite galaxies (on average 4.94 merging satellites/MW-like progenitor are found at $z = 3$), which are also modeled by composite stellar+DM potentials.

2.2. Initial conditions for globular clusters

Once the gravitational potentials of the MW progenitor galaxies and their satellites are defined at high redshift, we describe how a GC system was assigned to each of these galaxies. The initial number of GCs in galaxies is defined by the relation from Burkert & Forbes (2020), which accounts for the star formation rate and the efficiency of GC formation:

$$\langle \log N_{\text{GC}} \rangle = -9.58 \pm 1.58 + (0.99 \pm 0.13) \log \frac{M_{\text{vir}}}{M_\odot}. \quad (1)$$

This relation depends on the DM mass of the galaxies at the redshift where the clusters are tagged. We generate a GC distribution at $z = 2$ in the progenitors of the MW for the in-situ population, and at $z = 3$ in the progenitors of merging galaxies for the ex-situ population. Given that the stellar halo was likely accreted between 9 and 11 Gyr ago (Di Matteo et al. 2019; Mackereth & Bovy 2020) and cosmological simulations predict MW mass reaches its asymptotic value 9–10 Gyr ago (Diemand et al. 2007;

¹ Available at <https://www.tng-project.org/>

² Available at <https://github.com/jobovy/galpy>

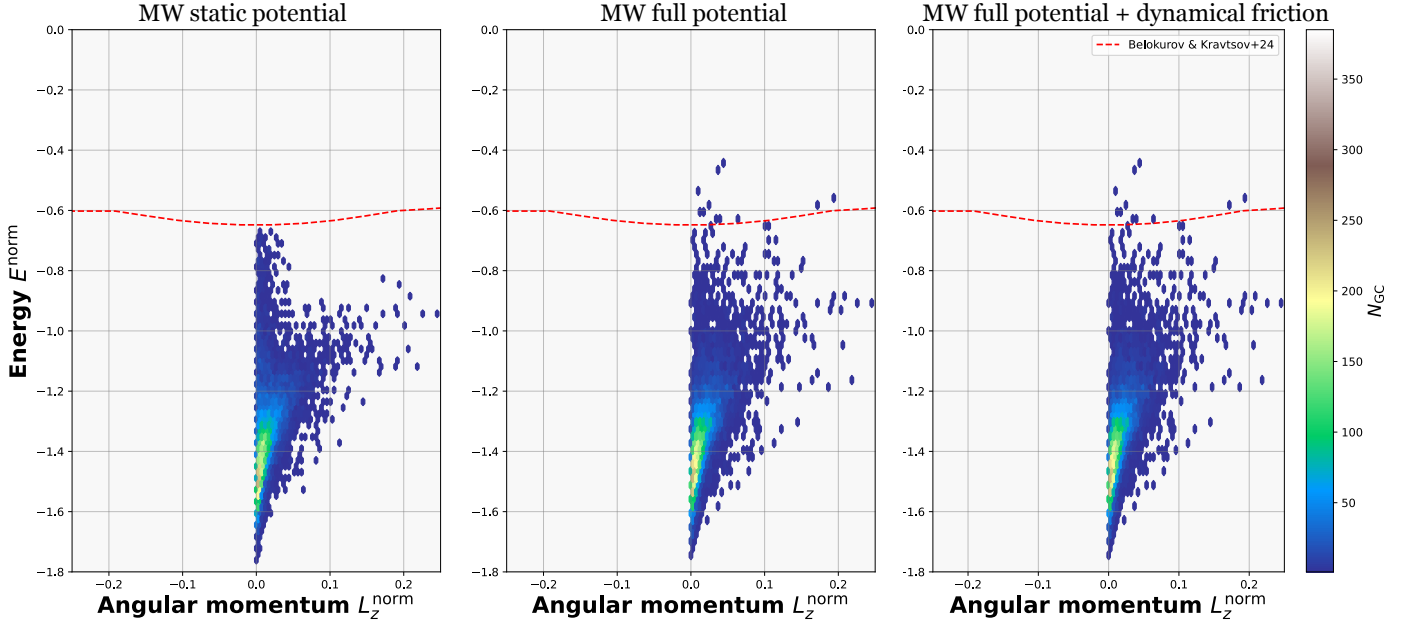


Fig. 3. *In-situ populations at $z = 0$:* Normalized total energy as function of the normalized z -component of the angular momentum at $z = 0$ for all our in-situ GCs for the 198 MWs with three different descriptions for the MW environment (see section 2.1 for the definitions of potentials). The hexagonal bins represent at least 1 GC. The red dashed line represents the (Belokurov & Kravtsov 2024) limit.

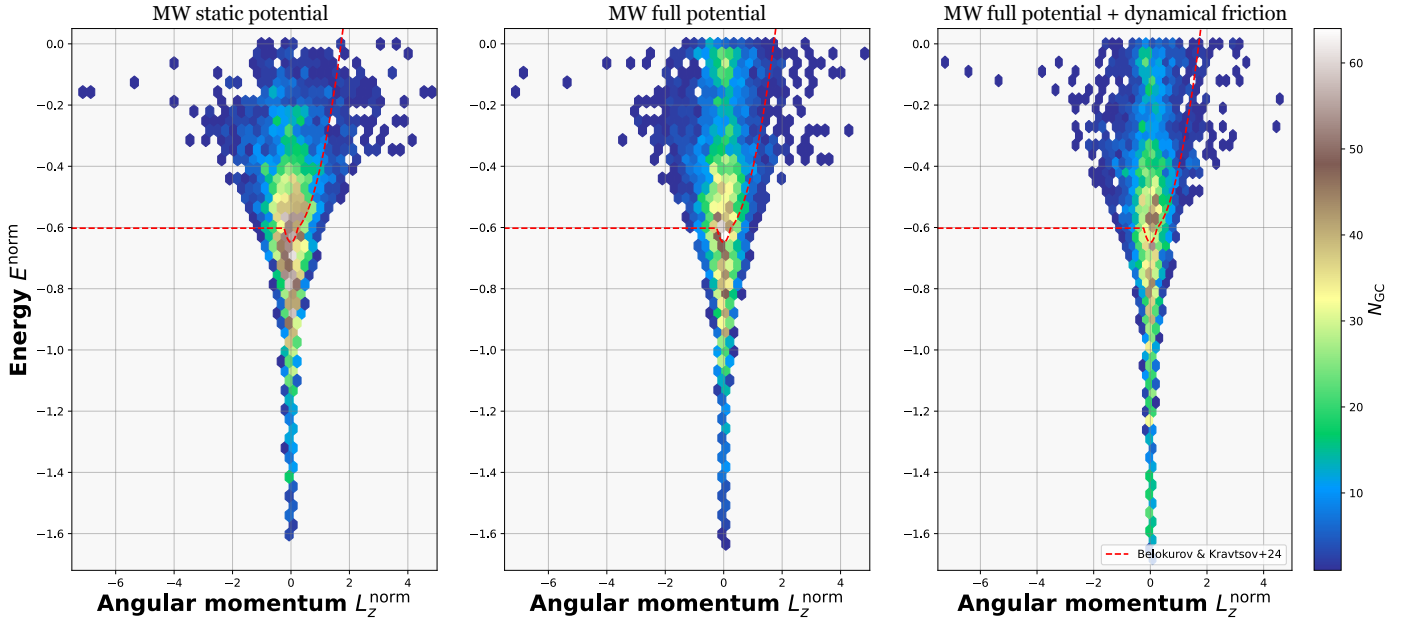


Fig. 4. *Ex-situ populations at $z = 0$:* As in Fig but for our ex-situ GCs for the 198 MWs.

(Lux et al. 2010; Diemer et al. 2013), we estimate that the number of GCs calculated from the above relation is more realistic at $z = 2$ than at $z = 3$ in our model. $z = 2$ is an observationally motivated choice to assign GC systems in order to reproduce the observed stellar mass–GC number relation at $z = 0$. In cases where our satellites were not yet formed at $z = 3$ in the simulation, we tag the GCs at a lower redshift.

Next, in each sufficiently massive galaxy ($M_{\text{DM}} > 5 \times 10^9 M_{\odot}$) to ensure that at least one GC is present, we derive the initial positions and velocities of in-situ GCs from stellar distribution functions based on our sample of progenitor galaxies and ex-situ GCs from those of the TNG50 stars. For in-situ populations, we

use the publicly available code **AGAMA**³ to construct equilibrium galaxy models composed of a stellar bulge and a DM halo for our $z = 2$ MW progenitor (Vasiliev 2019). For each system, a self-consistent potential is computed via iterative modelling, from which a phase-space distribution of stellar particles is sampled. We then select a subset of particles within the stellar half-mass radius to represent in-situ GCs. The advantage of this approach is that it allows us to generate a sufficient number of GCs with angular momentum $L_z > 0.6 L_{\text{circ}}$, where L_{circ} is the angular momentum of a circular orbit at the same energy, in order to impose a disc-like initial configuration for the in-situ population. Indeed,

³ Available at <https://github.com/GalacticDynamics-Oxford/Agama>

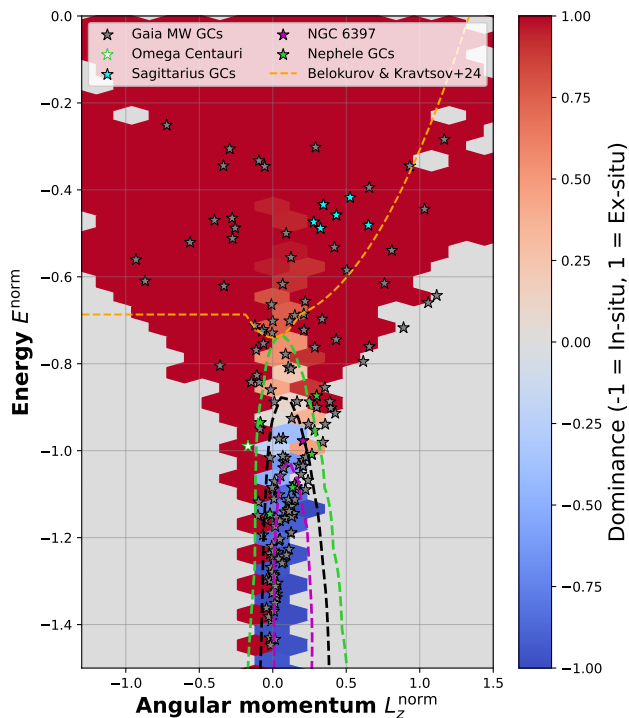


Fig. 5. Comparison with Gaia MW GCs: Normalized total energy as function of the normalized z-component of the angular momentum at $z = 0$ for both in-situ and ex-situ GCs for the 198 MWs in the full MW potential + dynamical friction. The decision boundaries in dashed lines corresponding to probabilities of 0.05 (magenta), 0.5 (black), and 0.95 (green) are plotted to illustrate the separation between the two populations. Nephelae GCs are the six GCs brought by the progenitor of Omega Centauri identified by Pagnini et al. (2025a). The 0.5 boundary results in an error of 1.35% for in-situ GCs and 11.2% for ex-situ GCs. The extreme boundary at 0.95 (0.05) excludes 99.72% (97.3%) of in-situ (ex-situ) GCs while identifying 81.2% (76.4%) of ex-situ (in-situ) GCs. We establish that between these two limits, distinguishing the two populations is not feasible with previous methods due to the presence of a mixing zone.

the stellar sample at $z = 2$ in the TNG50 MW analogues does not contain enough star particles with $L_z > 0.6L_{\text{circ}}$ to populate the number of clusters required by Burkert & Forbes (2020). For ex-situ GCs, we only randomly select N_{GC} stars within the stellar half-mass radius of the galaxies. Therefore, our accreted GCs inherit the positions and velocities of the stars present in TNG50 satellites.

We assign a mass of $10^6 M_{\odot}$ and a half-mass radius of 10 pc to all GCs. This arbitrary choice is motivated by the fact that it allows us to recover the typical mass ($\sim 10^5 M_{\odot}$) and size values of MW GCs today rather than modeling the full mass spectrum of MW clusters. In fact, a mass of $6 \times 10^6 M_{\odot}$ corresponds to the upper limit of the stellar mass of Galactic GCs 12 Gyr ago (Baumgardt et al. 2019). Moreover, dynamical friction for in-situ GCs is inefficient over our timescale (11 Gyr) due to the large mass ratio between the MW's enclosed mass and the GC masses. While the half-mass radius is kept constant during our orbit integrations, we account for mass loss over time (Kruijssen et al. 2011). For this mass loss model, we adopted the following parameters: $\gamma = 0.62$ and $t_{0,\odot} = 21.3$ Myr, which correspond to clusters with masses around $\sim 10^6 M_{\odot}$. Therefore, with these parameters, we aim to describe an average behavior over time.

We point out the limitations of the adopted mass loss model, particularly its inability to account for GC mass loss driven by rapidly varying tidal fields during disk crossings or interactions with molecular clouds. As highlighted by Renaud (2020b), such processes are not captured in current cosmological simulations due to insufficient spatial resolution, and their omission could significantly affect predictions of GC mass evolution.

2.3. Orbital integrations

To integrate the orbits of GCs, we require not only the MW gravitational potentials at different epochs (as described in section 2.1), but also the orbits of all merging satellites relative to the MW-like galaxy. This is essential because each satellite's trajectory affects the evolution of the GC system in two key ways: by perturbing the spatial distribution of the in-situ clusters, and by guiding the accreted clusters during their infall and subsequent evolution within the host galaxy.

The orbits of the satellite galaxies are also retrieved from TNG50. However, we re-integrate these merging satellite orbits into our MW potentials by taking into account dynamical friction, both to improve the time resolution of orbits that are sometimes highly jagged in the simulation due to non-linear time evolution, and to incorporate them as "moving potentials" in our full MW potential. Figure A.1 compares the orbits of several satellites in an MW and the orbits we re-integrated for the reasons mentioned above. TNG50 provides 100 snapshots from $z = 20$ and 0, distributed non-uniformly in time. In all our realizations, the satellite galaxy potentials evolve in both mass and size over time, as expected from cosmological evolution. As they orbit MW galaxies, satellites are subject to dynamical friction, which gradually alters their trajectories. The time-dependent masses and half-mass radii of the satellites are extracted directly from the TNG50 simulation and are used to compute the corresponding dynamical friction forces exerted by the MW-like host. We adopt the Chandrasekhar dynamical friction formula, as implemented in galpy, which closely follows the prescription of Petti et al. (2016).

For GCs, we include both dynamical friction and mass loss in the orbital integrations. At each update of the MW potential, GC mass loss is computed using the model of Kruijssen et al. (2011), which includes contributions from stellar evolution, two-body relaxation, and tidal shocks. In orbital integrations, mass loss impacts the dynamics of the GCs only in the presence of dynamical friction, which is updated at each change of potential and takes into account the mass loss of GCs. The evolution of mass and structural parameters of the host galaxy accounts for the influence of merging satellites, modeled as moving potentials, and includes dynamical friction exerted by the host galaxy on the GCs. We refer to this description as the **"MW full potential + dynamical friction"**. For comparison, we also consider two alternative potential models: one where the MW full potential evolves over time but without including dynamical friction, and another where the MW potential is fixed without dynamical friction and corresponds to the TNG50 snapshot at $z = 0$. We refer to these two configurations as **"MW full potential"** and **"MW static potential"**, respectively. In our approach, we distinguish between the orbital integrations of ex-situ and in-situ GCs. Specifically, ex-situ GCs first evolve within the potential of their progenitor galaxy, which is a merging galaxy of the MW, and are later accreted by the MW, thus evolving in its potential (see Figure 1). During the initial phase, ex-situ GCs orbit within the reference frame of their satellite galaxy until their orbital energy becomes positive ($E > 0$). Once this condition

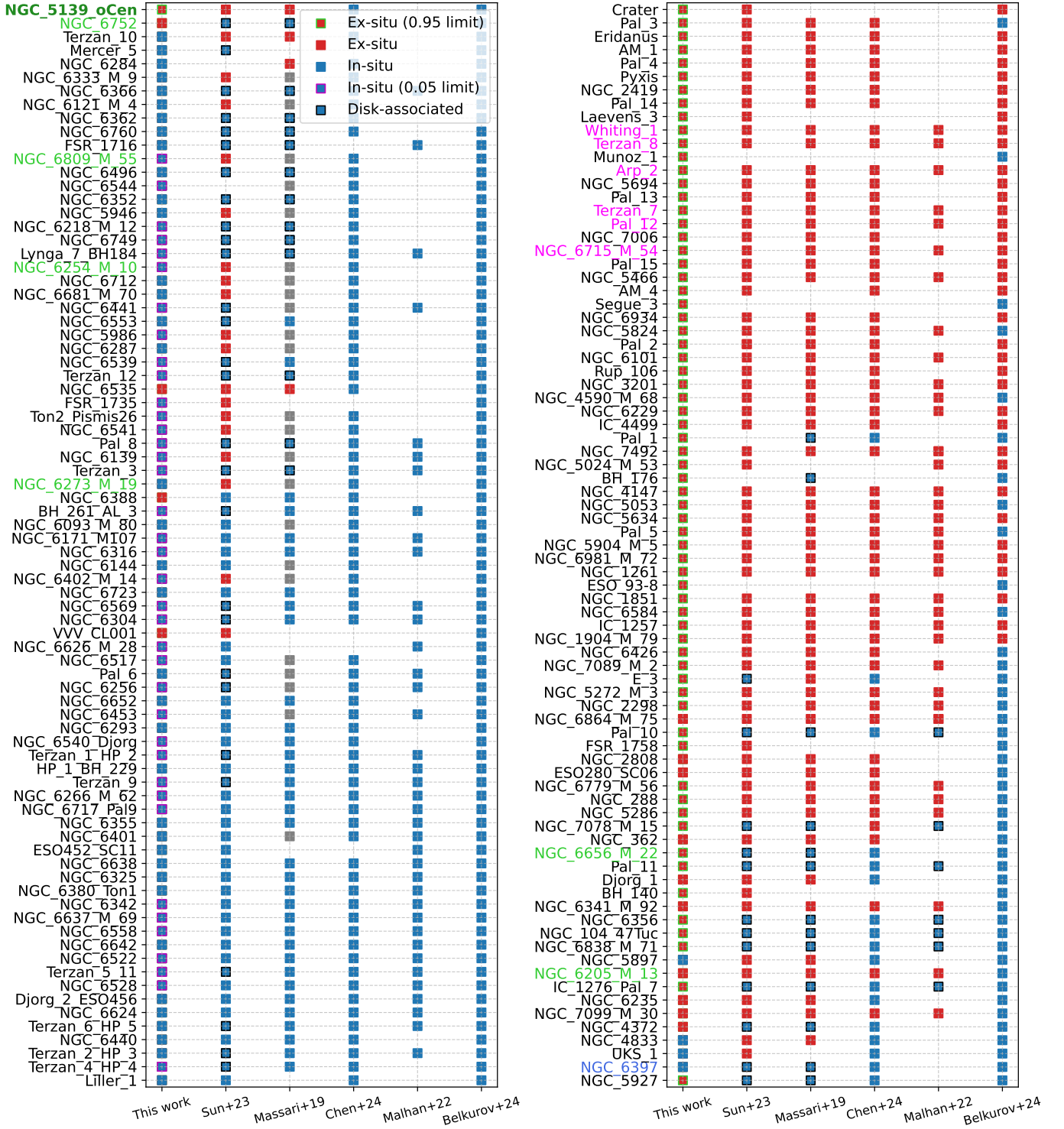


Fig. 6. *Origin of MW GCs:* Each point represents a GC and is color-coded according to its origin. GCs are sorted from the most to the least bound in energy. In-situ clusters (blue) with black edges are those associated with the MW disk by other studies. We also highlight the six GCs still associated with the Sagittarius dwarf galaxy (magenta), NGC 6397 (blue), and Omega Centauri (bold green), along with its six candidate clusters identified by [Pagnini et al. \(2025a\)](#) (light green). [Massari et al. \(2019\)](#) GCs whose origin remains unidentified but which have been classified as 'low-energy' GCs are in grey.

is met, GCs are transferred to the MW's reference frame while maintaining the moving potential of the satellite galaxy if it has not yet merged. This procedure is necessary because the calculation of dynamical friction from a galaxy is only possible within that galaxy's reference frame in *galpy*. Once accreted at a given

redshift, ex-situ GCs evolve like in-situ GCs in the full MW potential. We have verified that once tagged, both ex-situ and in-situ GCs remain bound to their host galaxies ($E < 0$). We have checked that the distribution of in-situ GCs are bound to the various progenitors of the MW by computing the normalized total

energy versus normalized z -component of the angular momentum space at $z = 2$.

To compute the orbits, we used a fast C integrator, `dop853c`, implemented in `galpy`. This is an explicit Runge–Kutta method of order 8(5,3), which offers high accuracy and efficiency for integrating complex dynamical systems. Our orbital-time resolution is set to 2 Myr (500 time steps per Gyr), which is sufficient to obtain smooth and accurate orbits over these time scales. We apply this procedure to our full sample of 198 MW analogues from TNG50. Regarding the computational performance of our model, orbital integrations between $z = 3$ and 0 for our entire sample take between 1 and 440 CPU hours. This variation depends on the potential description, as dynamical friction significantly slows down the code.

3. Results

In the following, we only consider ex-situ GCs with negative total energy at $z = 0$, i.e. those that remain gravitationally bound to the MW, since we identified a small fraction of ex-situ GCs that are unbound at $z = 0$, representing 2% and 10% of the ex-situ population in the static and full potential + dynamical friction models, respectively. In fact, during their escape from the satellite potential, either due to satellite evolution or merger, these GCs have sufficient energy to not be trapped within the MW potential. A smaller number of wandering GCs in the static potential is found, as expected, since it is described by the most massive MW potential at $z = 0$. Then, in order to fairly compare the populations of our 198 MW analogues, which have different mass distributions as shown in the Figure 2, we chose to normalize ($E - L_z$) space.

In our analysis, the energy E is normalized by the energy of a circular orbit at the stellar half-mass radius, $E_{\text{circ}}(r_{\text{hm}})$. r_{hm} provides a physically meaningful scale for two main reasons: (i) it approximately marks the transition between the in-situ and ex-situ GC populations, as in-situ clusters typically form within this radius; and (ii) this radius is directly measurable in observations, enabling robust comparisons with simulations. The angular momentum L_z is normalized by $\sqrt{GM_{\text{tot}}/r_{\text{hm}}}$, where M_{tot} is the total mass of the host galaxy, including DM. This normalization cap-

tures the influence of the global gravitational potential on the orbital dynamics of GCs, particularly for those on wide orbits. It also allows for meaningful comparisons between systems of different total mass while maintaining a common baryonic scale via r_{hm} .

We followed the dynamics of 17,726 GCs, including 13,339 in-situ and 4,387 ex-situ, across three different MW potential descriptions: MW static potential, MW full potential, and MW full potential + dynamical friction (see Section 2.1 for the definitions of potentials). Thanks to our mass-loss implementation from Kruijssen et al. (2011), we can determine the final mass of the GCs, especially those that have survived. The following plots (Figure 3, 4 and 5) show the population of surviving GCs. On average, only 0.01% of the ex-situ GCs are destroyed, compared to 35% of the in-situ ones. This directly echoes a similar result from Renaud et al. (2017b), who found that in-situ GCs experience significantly stronger tidal forces than their accreted counterparts. Assuming an initial GC mass of $10^6 M_{\odot}$, we observe that, by $z = 0$, the mass of surviving clusters spans a wide range from $3.2 \times 10^3 M_{\odot}$ up to $5 \times 10^5 M_{\odot}$. Interestingly, the ex-situ population typically retains a mass close to its initial value, highlighting their relative resilience to tidal disruption in MW-like environments.

3.1. In-situ globular clusters

Figure 3 shows that the evolution of the potential and dynamical friction have a negligible effect on the distribution of in-situ GCs in the $E - L_z$ space. As a matter of fact, the evolution of the potential will stretch some GCs toward higher energies, but most clusters are concentrated at $E < 1.2 E_{\text{circ}}(r_{\text{hm}}^*)$. We observe no variation in this dense cluster region across the three descriptions. Since the potential evolves gradually, GCs can simply adjust adiabatically without significant diffusion in the $E - L_z$ plane. This is expected, as the mass growth of the MW in CDM framework occurs relatively smoothly. Regarding dynamical friction, its negligible impact is also expected, given that it is generally negligible in MW-like galaxies due to the large mass ratio between the enclosed MW mass and GC mass. Moreover, Figure 3 clearly shows that it is highly unlikely to find in-situ GCs at $E > 0.7 E_{\text{circ}}(r_{\text{hm}}^*)$.

3.2. Ex-situ globular clusters

Figure 4 depicts that the GC distribution is more spread out in energy in the full MW potential compared to the static potential, as the evolving potential is less massive and can sustain orbits at higher energies than the MW potential at $z = 0$. Dynamical friction slightly reduces the GC density distribution in the high-energy range. It also confirms the presence of an overlap between the two populations in MW-like galaxies, occurring below an energy threshold of $E < 0.7 E_{\text{circ}}(r_{\text{hm}}^*)$, as ex-situ clusters span the entire energy range. We emphasize that ex-situ GCs are present across the full energy range, invalidating the limit proposed by Belokurov & Kravtsov (2024); Massari et al. (2019); Callingham et al. (2022); Chen & Gnedin (2024). In practical terms, this threshold can at best be used to exclude the in-situ population. Besides, we note that very few ex-situ clusters are found below approximately $1.25 E_{\text{circ}}(r_{\text{hm}}^*)$.

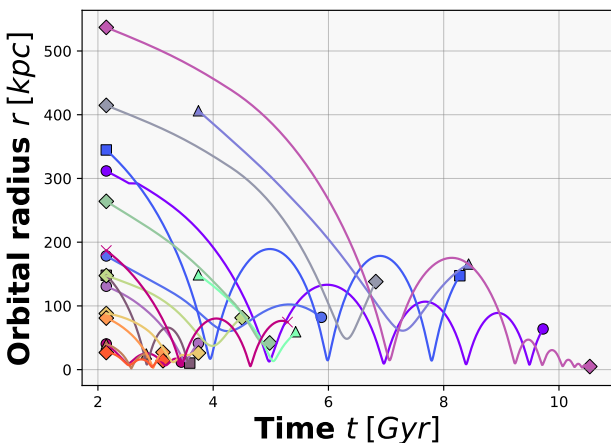


Fig. 7. Orbital evolution of merging satellites from five MW galaxies (IDs 342447, 372754, 372755, 388544 and 392277) in our sample, described by a full potential + dynamical friction. The points mark the formation and merger times of the satellites in the TNG50 simulation.

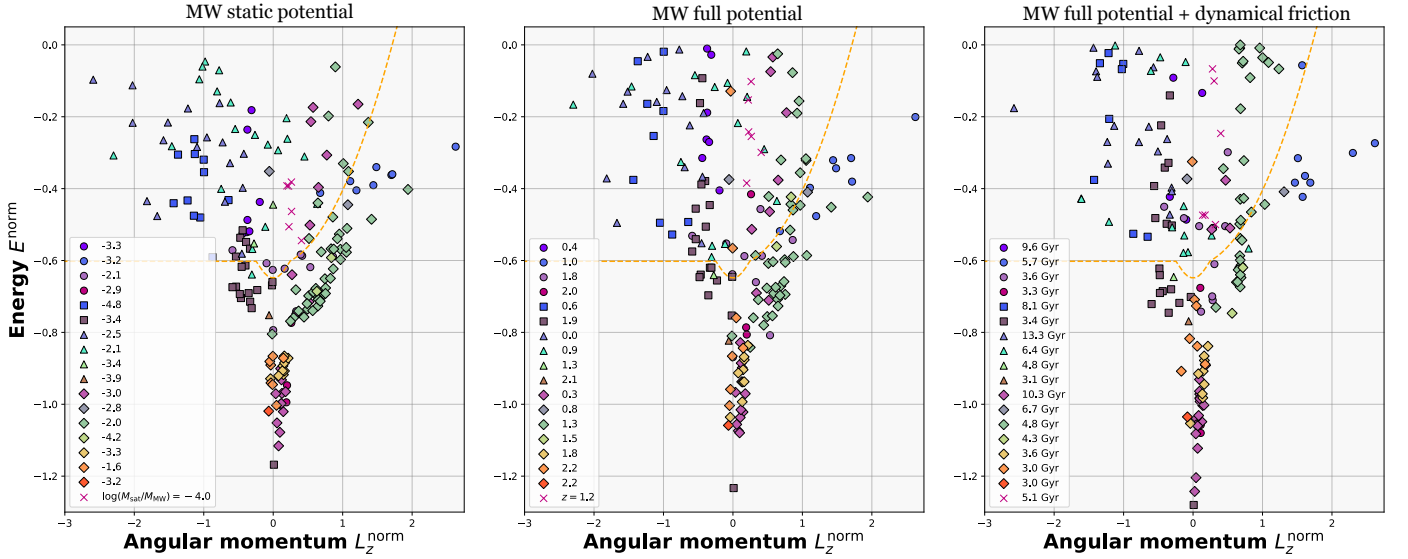


Fig. 8. $E - L_z$ decoherence of ex-situ GC groups due to evolving MW potentials and dynamical friction: Normalized total energy as function of the normalized z -component of the angular momentum at $z = 0$, colour-coded according to their associations with satellites from the same five MW galaxies shown in Figure 7. The captions provide information on the mass ratio between the satellite galaxy and the MW at the time of the merger (left panel), the redshift (middle panel), and the merger time (right panel).

3.3. Comparison with Gaia MW GCs

Figure 5 compares our results in the full MW potential, including dynamical friction, with the distribution of GCs in the MW as provided by Gaia (Vasiliev & Baumgardt 2021) in the normalized space $E - L_z$. For the observed clusters, we assumed the potential from McMillan (2017), a multi-component analytic model of the MW calibrated to reproduce a wide range of observables. This MW potential has an stellar half-mass radius of 4.6 kpc. For our simulated clusters, we used a hexagonal density plot, where the color represents the dominant origin of the GCs (ex-situ or in-situ). Dominance is defined as the ratio $(N_{\text{ex-situ}} - N_{\text{in-situ}}) / (N_{\text{ex-situ}} + N_{\text{in-situ}})$, where $N_{\text{ex-situ}}$ and $N_{\text{in-situ}}$ are the number of ex-situ and in-situ GCs, respectively. Red indicates a predominance of ex-situ clusters (+1), while blue corresponds to in-situ clusters (-1). As highlighted in previous Figures 3 and 4, our dominance map confirms that ex-situ clusters dominate for $E > 0.7E_{\text{circ}}(r_{\text{hm}})$, while in-situ clusters dominate for $E < 1.25E_{\text{circ}}(r_{\text{hm}})$ for positive L_z . More specifically, our density map reveals that the dominance of ex-situ clusters extends up to $0.9; E_{\text{circ}}(r_{\text{hm}}^*)$, covering a larger fraction of the observed MW GCs distribution. Our results indicate that this boundary underestimates the number of ex-situ clusters: in fact, 55% of our ex-situ clusters fall below the Belokurov & Kravtsov (2024) threshold. Furthermore, if we were to adopt this boundary, our results suggest a misclassification of 28% of the clusters identified as in-situ, which are actually ex-situ. Finally, our results challenge simple energy threshold models, which we demonstrate to fail in clearly separating the two populations, and merely identifies a subset of ex-situ GCs. Moreover, Figure 5 clearly highlights that the real challenge lies in distinguishing the two populations below this energy threshold, where an overlap of both populations persists up to $E_{\text{circ}}(r_{\text{hm}}^*)$. The existence of this mixing zone is further supported by Andersson & Davies (2019), who predict that 50% of the globular clusters located in the central region of M31 were accreted.

3.4. Our new approach

This motivates our proposal for new boundaries that allow for the identification of a larger fraction of the ex-situ population while also capturing part of the in-situ population. We employed a Support Vector Machine (SVM)⁴, a supervised learning method, to classify the synthetic in-situ and ex-situ populations in the $E - L_z$ space. This algorithm aims to find an optimal hyperplane that separates the data in such a way as to maximize the margin between the two GC populations. We employed a radial basis function (RBF) kernel modeled by a squared exponential function, in order to transform the input space so that the data becomes linearly separable in a higher-dimensional feature space. The SVM was trained using this RBF kernel, with parameters chosen to minimize the classification error rate for both populations. In Figure 5, the decision boundaries corresponding to probabilities of 0.05, 0.5, and 0.95 are plotted to illustrate the separation between the two populations. The 0.5 boundary results in an error of 1.35% for in-situ GCs and 11.2% for ex-situ GCs. The extreme boundary at 0.95 (0.05) excludes 99.72% (97.3%) of in-situ (ex-situ) GCs while identifying 81.2% (76.4%) of ex-situ (in-situ) GCs. We establish that between these two limits, distinguishing the two populations is not feasible with previous methods due to the presence of a mixing zone. The in-situ boundary approximately corresponds to an energy thresholds of -1 . This is why, in Figure 6, where clusters are sorted from the least to the most bound in energy, Gaia MW GCs within the region of overlap are represented by squares (either in-situ (in blue) or ex-situ (in red)) without any border. We provide a new classification based on the 0.5 boundary established from the dynamics of our synthetic clusters within the full gravitational potential of 198 MW realizations. We used this threshold to identify ex-situ (in-situ) GCs, shown in red (blue) (see Figure 6). We also compare our updated classification of the MW GCs with previous studies (Massari et al. 2019; Malhan et al. 2022; Sun et al. 2023; Belokurov & Kravtsov 2024; Chen & Gnedin 2024). Since our ex-situ boundary lies at a lower energy threshold compared to

⁴ The implementation of the SVM was done using the scikit-learn library in python.

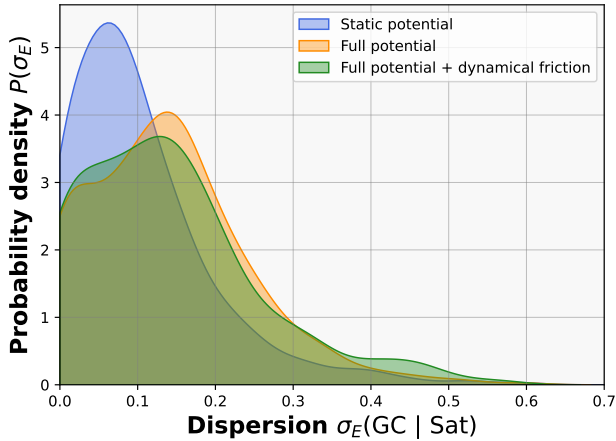


Fig. 9. Coherence loss in energy: Densité de probabilité $P(E)$ de la dispersion en énergie pour nos ex-situ GCs pour les 198 MWs à $z=0$. Nous calculons les dispersions d'énergie pour chaque groupe de GCs ex-situ. L'évolution du potentiel galactique induit une plus grande dispersion d'énergie pour les GCs originant de la même satellite.

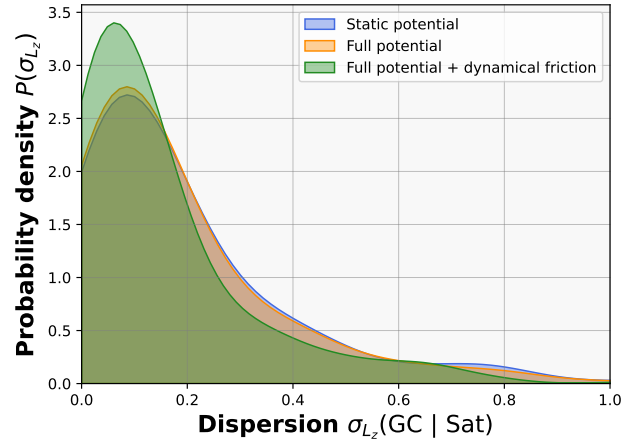


Fig. 10. Coherence loss in angular momentum: As in Fig but the la dispersion en angular momentum. Dynamical friction induces a more pronounced peak around a low L_z dispersion. This indicates that a portion of the globular clusters tends to remain grouped in L_z .

Belokurov & Kravtsov (2024), Sagittarius GCs are classified as ex-situ, as expected.

Among the 161 MW GCs, we identify 68 as ex-situ, 39 as in-situ, and 54 within the mixing zone. This why chemical abundance could provide additional constraints to disentangle these origins, as demonstrated by Pagnini et al. (2025b). If we adopt our decision threshold (0.5 boundary), meaning that the probability of belonging to either population is equal, we find an ex-situ to in-situ number ratio close to 1.03 (79 in-situ versus 82 ex-situ). This contrasts with Belokurov & Kravtsov (2024) and Chen & Gnedin (2024), who obtain reversed ratios of approximately 0.3 (124 in-situ versus 37 ex-situ) and 0.4 (94 in-situ versus 39 ex-situ), respectively, while Sun et al. (2023) reports a more balanced ratio of 1.2 (71 in-situ versus 88 ex-situ).

Figure 6 clearly shows that the 33 most tightly bound GCs (with lower energy than VVV_CL001) identified as in-situ are consistently found across all six studies. We also observe that our results for ex-situ GCs are in good agreement with the classifications from Massari et al. (2019); Malhan et al. (2022); Sun et al. (2023), except for a few clusters that were designated as in-situ in their classifications. Intriguingly, these discrepant GCs have all been identified as "Disk" GCs, meaning they exhibit properties such as low eccentricity (implying nearly circular orbits) and pericenter and apocenter radii similar to those of stars in the Galactic disk. This suggests that associating certain GCs with the disk based solely on these criteria may not be sufficiently constraining. Finally, all clusters located in the mixing zone (squares without any border in the left panel of Figure 6) have been classified as in-situ in previous studies, except for Sun et al. (2023). In their study, they identify a group of 26 GCs ('Pot') that are not associated with the bulge, the disk, or known major merger events. According to Sun et al. (2023), these clusters may originate from small accretion events and are therefore classified as ex-situ. Once again, the difficulty in distinguishing them from other GCs arises from their location in the region of overlap, where both populations overlap.

Concerning Omega Centauri (NGC 5139 in bold green), which is believed to be the nuclear star cluster of a galaxy accreted by the MW in the past, our analysis classifies it as ex-

situ in contrast to most results in the literature (see Figure 6). Furthermore, Pagnini et al. (2025a) identified six globular clusters brought by the progenitor of NGC 5139 by combining Gaia EDR3 data with chemical abundances from APOGEE DR17. NGC 6752, NGC 6656, NGC 6809, NGC 6273, NGC 6205, and NGC 6254 have a fraction of stars compatible with Omega Centauri greater than 60%. Our results confirm this prediction by identifying three of these clusters as ex-situ (with energies lower than or comparable to that of NGC 5139), while the remaining three lie in the mixing zone, with an uncertain but possibly ex-situ origin only for NGC 6273. Finally, we note that two of GCs identified as ex-situ (NGC 6752 and NGC 6656) are those with a compatibility greater than 80% with Omega Centauri.

Concerning another specific GC, NGC 6397, which is the second closest GC to the Sun, it is a low-mass and very compact cluster. Due to its proximity to the MW center, it should have experienced numerous tidal interactions, making it a strong candidate for the development of tidal tails. Moreover, Balbinot & Gieles (2018) estimated that it should have lost 72% of its initial mass. Actually, simulations of NGC 6397 generally predict prominent and extended tidal tails (kpc scale) around this cluster (Boldrini & Vitral 2021; Arnold & Baumgardt 2025). However, the existence of tidal tails around NGC 6397 remains debated. Leon et al. (2000) reported overdensities that were classified as unreliable due to uncertainties in the dust distribution around the cluster. More recently, Ibata et al. (2024) detected a possible tail extending over 18 degrees on the sky using Gaia data, but these findings were challenged by Boldrini & Vitral (2021), who did not detect any tidal tail. Ultimately, identifying potential stream members of NGC 6397 in Gaia data with precision remains a complex challenge. This is crucial to either confirm the absence of a stream, the presence of a sub-kpc stream, or the existence of a prominent stream as predicted by simulations assuming an in-situ evolution. Our results classify NGC 6397 (which has an energy level comparable to that of Omega Centauri) as in-situ, but this classification remains highly uncertain given its position near the 0.5 boundary (see Figure 5). Therefore, this does not rule out scenarios where either no tidal stream is present or only a sub-kiloparsec stream exists. Indeed, this aligns with the hypothesis proposed by Boldrini & Vitral (2021) that one possible

ex-situ scenario for this cluster is that it was initially embedded in a DM minihalo. In this scenario, the minihalo could have acted as a protective envelope, preventing the tidal stripping of stars while being gradually disrupted and removed over the course of the cluster's evolution. The combination of future releases from Gaia and Euclid will provide a better characterization of the tidal features of this cluster and further constrain its origin (Massari et al. 2024).

Finally, there is a group of 23 GCs whose origin remains unidentified but which have been classified as 'low-energy' GCs by Massari et al. (2019) due to their low energy and near-zero angular momentum. Our results indicate that this population has energies lying precisely in the mixing zone (see GCs in grey in Figure 6). The fact that these clusters fall within this energy range further complicates the determination of their origin and, more importantly, suggests the absence of a common progenitor. Besides, we find that 10 of them have an ex-situ origin.

In Figure A.2, we explore the impact of varying the mass choice on our results, which only affects the calculation of dynamical friction and mass loss. It was found that our results remain unchanged within a reasonable initial mass range for globular clusters ($0.5 - 5 \times 10^6 M_\odot$). Whereas increasing the mass has no effect, decreasing it slightly lowers the 0.05 boundary for the in-situ GCs.

3.5. $E - L_z$ decoherence of ex-situ GC groups

Our final investigation focuses on the distribution of ex-situ GC groups originating from the same satellite, still in phase space $E - L_z$, as shown in Figure 8, for our three descriptions of the MW potential over time (see Section 2.1 for definitions of potentials). An important result is that GCs from the same satellite can have different energies, as well as both positive and negative z-components of angular momentum. Furthermore, the boundary proposed by Belokurov & Kravtsov (2024) can separate GCs originating from the same satellite. Upon visual inspection of Figure 8, we observe that the evolving potential tends to break the coherence of GC groups from the same satellite across five MW galaxies in our sample, whose orbits are provided in Figure 7. This decoherence manifests as a diffusion of GC groups towards higher energies, due to the changes in the potential experienced by the ex-situ GCs. Unlike in-situ GCs, ex-situ globular clusters take longer to adapt to variations in the gravitational potential, resulting in an increase in their energy dispersion. Interestingly, the addition of dynamical friction tends to accelerate this adaptation process, as we observe a slight decrease in the energies of the GCs. A notable effect initiated by dynamical friction is its tendency to align the angular momentum of GCs from the same satellite. Indeed, dynamical friction is a process that removes angular momentum and orbital energy, driving the GCs towards more radial orbits.

To confirm these behaviors across our sample of 198 MWs, we calculate the energy and angular momentum dispersions for each ex-situ GC group at $z = 0$, as shown in Figures 9 and 10, respectively. In Figure 9, for the static potential case (blue), we observe a pronounced peak towards small dispersions. When we account for an evolving potential (orange), the distribution shifts slightly towards higher values, with a flattening of the main peak. This suggests that the evolution of the galactic potential induces a greater energy dispersion for GCs originating from the same satellite. This confirms that variations in the potential well alter the orbits of accreted GCs, as visually observed in the example in Figure 7. The addition of dynamical friction (green) slightly reduces the energy dispersion. As seen in Figure 9, the progres-

sive energy loss of the globular clusters due to dynamical friction slightly narrows the energy gap between them. In Figure 10, the inclusion of an evolving potential does not affect the L_z distribution of ex-situ GCs at $z = 0$, whereas dynamical friction induces a more pronounced peak around a low L_z dispersion. This indicates that a portion of the globular clusters tends to remain grouped in L_z . Once again, this is expected, as dynamical friction removes angular momentum from the orbiting GCs.

4. Caveats

In this work, as a first approximation, we tagged ex-situ GCs at $z = 3$ in satellite galaxies and in-situ GCs at $z = 2$ in the MW progenitors. To increase realism, future studies will need to tag clusters at all redshifts, based, for example, on a formation efficiency parameter derived from gas and stellar quantities resolved in the simulation (e.g., as in Pfeffer et al. (2018); Reina-Campos et al. (2022); Grudić et al. (2023); Newton et al. (2024); Rodriguez et al. (2023)). However, high-resolution or zoom-in simulations, which typically generate a maximum of 20 MW-like galaxies, are required to calculate these parameters because a gas resolution of the order of 1-10 pc is necessary to obtain reliable information on gas pressure and star formation, which enhance the formation of globular clusters. Although TNG50 is not as precise, with an average cell size of 70-140 pc in the star-forming regions of galaxies, it allows us to access approximately 200 MW-like galaxies (Pillepich et al. 2019). Although our approach is statistically consistent with the estimated ages of all GCs in the MW, it is not consistent with younger clusters with lower masses ($10^{4-5} M_\odot$). Moreover, tagging clusters at lower redshifts will increase the population of clusters that survive in environments like those of MW-type galaxies. In the same spirit, a tagging method based on a formation efficiency parameter using gas and stellar quantities would provide a more realistic mass for the GCs. However, the goal of our initial approach was to model the average behavior of clusters with masses on the order of $10^6 M_\odot$. In our analysis, we only consider satellite galaxies with stellar masses above $10^7 M_\odot$. However, lower-mass galaxies, which are not resolved in this study, may be highly efficient sites of GC formation, as indicated by recent results from the EDGE simulations (Taylor et al., submitted). This limitation clearly motivates future investigations using zoom-in simulations that can better resolve low-mass DM halos and their contribution to the GC population.

Another point to improve our approach is to include the presence of the MW's disk, particularly to account for its dynamical impact on the in-situ population. In this work, our MWs are only modeled with DM and stellar spherical components. Although these components have been studied in TNG50, they were not cataloged in the same way as the other components for our MW sample to be incorporated into our study (Sotillo-Ramos et al. 2022). An alternative to avoid imposing fixed structures (Hernquist bulge, exponential disk, NFW DM halo) and breaking this idealized modeling of the MW via a spherical potential is to use methods like AGAMA (Vasiliev 2019). This would allow us to build a self-consistent galactic potential based on the galaxy's full distribution function, including non-trivial effects such as local density variations.

5. Conclusion

In this work, we presented a new cosmological post-processing framework to study the hierarchical assembly of GCs in MW-like galaxies. By coupling the cosmological hydrodynamical

simulation TNG50 with orbital integrations using `galpy`, and by including realistic treatments of dynamical friction and mass loss, we followed the evolution of 18,000 GCs—both in-situ and ex-situ—across 198 MW analogues from redshift $z = 3$ to $z = 0$. This approach allowed us to explore, for the first time at this statistical scale, how these two GC populations dynamically evolve and mix within time-evolving galactic potentials shaped by mergers and mass accretion.

We find that in-situ GCs predominantly occupy a well-defined region of the normalized energy–angular momentum $E-L_z$ space, remaining tightly bound and dynamically cold even in the presence of an evolving MW potential. In contrast, ex-situ GCs span a broader range in energy and angular momentum, reflecting their varied accretion histories. Importantly, we confirm the existence of a significant mixing zone below the energy threshold $E < 0.7 E_{\text{circ}}(r_{\text{hm}}^*)$, where both in-situ and ex-situ GCs overlap. This undermines previous attempts to cleanly separate the two populations using only the integral of motions via a single cut in energy, which based on our models will not be able to reproduce a large fraction of ex-situ clusters and will misclassify many in-situ ones.

We proposed a new classification scheme, which allows a probabilistic separation of the two populations and highlights the limitations of binary thresholds. Applying this scheme to the observed MW GC system using Gaia kinematics, we identify 82 GCs as ex-situ, 79 as in-situ (see Figures 5 and 6). This revised classification leads to a more balanced in-situ to ex-situ ratio. Notably, we confirm the ex-situ nature of Omega Centauri and its associated group of GCs, as well as the Sagittarius GCs, and identify potential misclassifications among clusters previously associated with the Galactic disk.

Explicit modeling of mass loss during orbital integration, using the prescription of Kruijssen et al. (2011), allowed us to find that in-situ GCs experience significantly stronger tidal disruption, leading to an average survival fraction of only $\sim 65\%$, while ex-situ GCs are more resilient, with a destruction rate below 1%. As a result, surviving ex-situ clusters retain masses closer to their initial values, while many in-situ clusters are heavily stripped, in agreement with Renaud et al. (2017b). This asymmetry in mass loss could provide a key additional constraint in disentangling the two populations, as well as shedding light on the origin of the extremely metal-poor stellar streams identified by Ibata et al. (2024), which have not been linked to any known globular cluster progenitor. Our results point toward a possible scenario in which these streams are the remnants of a disrupted, ancient population of in-situ GCs, destroyed during the early phases of the Galaxy’s evolution.

Furthermore, we studied the loss of orbital coherence among GC groups accreted from the same satellite. We find that the evolving MW potential, combined with dynamical friction, progressively erases the initial correlations in $E - L_z$ space. This challenges the assumption that GCs accreted from the same progenitor should remain kinematically coherent, even in action space, and calls for caution when associating groups of clusters with past accretion events.

Overall, our results show that the dynamical separation of GC populations requires modeling their full cosmological context, including satellite orbits, potential evolution, and external GC evolution. Our method bridges the gap between large-scale statistical studies and the dynamical modeling of individual clusters, offering new insights into the assembly history of the MW. Future improvements will involve tagging GCs based on more physically motivated formation efficiencies, including baryonic structures like the MW disk, and using higher-resolution MW

simulations such as VINTERGATAN (Agertz et al. 2021) and HESTIA Libeskind et al. (2020) to refine GC initial conditions. Such developments will further enhance our ability to disentangle the complex origin of the Galactic globular cluster system in the Gaia era, as well as with Euclid (Euclid Collaboration et al. 2025; Saifollahi et al. 2025a,b).

6. Data Availability

The data underlying this article is available through reasonable request to the author. The code and GC data will be available at the following URL: <https://github.com/Blackholan>.

7. Acknowledgements

PB acknowledges funding from the CNES post-doctoral fellowship program. PB thanks members of the Euclid working group, "Extragalactic globular clusters", for contributing with useful comments in the early stages of this project. PB wants to express his gratitude to Misha Haywood for suggesting a more impactful title. The IllustrisTNG simulations were undertaken with compute time awarded by the Gauss Centre for Supercomputing (GCS) under GCS Large-Scale Projects GCS-ILLU and GCS-DWAR on the GCS share of the supercomputer Hazel Hen at the High Performance Computing Center Stuttgart (HLRS), as well as on the machines of the Max Planck Computing and Data Facility (MPCDF) in Garching, Germany.

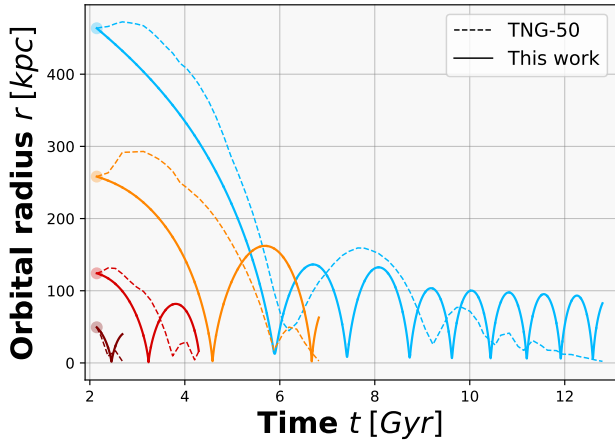


Fig. A.1. Orbits of merging satellites from TNG50 and from our orbital integrations in our analytic MW potential. We have re-integrated satellite orbits both to improve the time resolution of orbits that are sometimes highly jagged in TNG50 due to non-linear time evolution, and to incorporate them as "moving potentials" in our full MW potential.

Appendix A: Appendix

References

- Agertz, O., Renaud, F., Feltzing, S., et al. 2021, *MNRAS*, 503, 5826
Amarante, J. A. S., Debattista, V. P., Beraldo e Silva, L., Laporte, C. F. P., & Deg, N. 2022, *ApJ*, 937, 12
Andersson, E. P. & Davies, M. B. 2019, *MNRAS*, 485, 4134
Andersson, E. P., Mac Low, M.-M., Agertz, O., Renaud, F., & Li, H. 2024, *A&A*, 681, A28
Arnold, A. D. & Baumgardt, H. 2025, *MNRAS*, 537, 1807
Balbinot, E. & Gieles, M. 2018, *MNRAS*, 474, 2479
Baumgardt, H., Hilker, M., Sollima, A., & Bellini, A. 2019, *MNRAS*, 482, 5138
Beasley, M. A. 2020, in *Reviews in Frontiers of Modern Astrophysics: From Space Debris to Cosmology*, ed. P. Kabáth, D. Jones, & M. Skarka, 245–277
Bekki, K. & Freeman, K. C. 2003, *MNRAS*, 346, L11
Belokurov, V. & Kravtsov, A. 2023, *MNRAS*, 525, 4456
Belokurov, V. & Kravtsov, A. 2024, *MNRAS*, 528, 3198
Binney, J. & Tremaine, S. 2008, *Galactic Dynamics: Second Edition*
Boldrini, P. & Vitral, E. 2021, *MNRAS*, 507, 1814
Bovy, J. 2015, *ApJS*, 216, 29
Bullock, J. S. & Johnston, K. V. 2005, *ApJ*, 635, 931
Burkert, A. & Forbes, D. A. 2020, *AJ*, 159, 56
Callingham, T. M., Cautun, M., Deason, A. J., et al. 2022, *MNRAS*, 513, 4107
Carraro, G. & Lia, C. 2000, *A&A*, 357, 977
Chen, Y. & Gnedin, O. Y. 2023, *MNRAS*, 522, 5638
Chen, Y. & Gnedin, O. Y. 2024, *The Open Journal of Astrophysics*, 7, 23
Cooper, A. P., Cole, S., Frenk, C. S., et al. 2010, *MNRAS*, 406, 744
Creasey, P., Sales, L. V., Peng, E. W., & Sameie, O. 2019, *MNRAS*, 482, 219
Deng, Y., Li, H., Liu, B., et al. 2024, *A&A*, 691, A231
Di Matteo, P., Haywood, M., Lehnert, M. D., et al. 2019, *A&A*, 632, A4
Diemand, J., Kuhlen, M., & Madau, P. 2007, *ApJ*, 657, 262
Diemer, B., More, S., & Kravtsov, A. V. 2013, *ApJ*, 766, 25
Doppel, J. E., Sales, L. V., Nelson, D., et al. 2023, *MNRAS*, 518, 2453
Dubois, Y., Beckmann, R., Bournaud, F., et al. 2021, *A&A*, 651, A109
Euclid Collaboration, Voggel, K., Lançon, A., et al. 2025, *A&A*, 693, A251
Forbes, D. A. & Bridges, T. 2010, *MNRAS*, 404, 1203
Gaia Collaboration, Brown, A. G. A., Vallenari, A., et al. 2021, *A&A*, 649, A1
Gaia Collaboration, Helmi, A., van Leeuwen, F., et al. 2018, *A&A*, 616, A12
Grudić, M. Y., Hafen, Z., Rodriguez, C. L., et al. 2023, *MNRAS*, 519, 1366
Halbesma, T. L. R., Grand, R. J. J., Gómez, F. A., et al. 2020, *MNRAS*, 496, 638
Helmi, A. 2020, *ARA&A*, 58, 205
Hernquist, L. 1990, *ApJ*, 356, 359
Ibata, R., Malhan, K., Tenachi, W., et al. 2024, *ApJ*, 967, 89
Jean-Baptiste, I., Di Matteo, P., Haywood, M., et al. 2017, *A&A*, 604, A106
Khoperskov, S., Minchev, I., Libeskind, N., et al. 2023a, *A&A*, 677, A89
Khoperskov, S., Minchev, I., Libeskind, N., et al. 2023b, *A&A*, 677, A90
Kim, J.-h., Ma, X., Grudić, M. Y., et al. 2018, *MNRAS*, 474, 4232
Kravtsov, A. V. & Gnedin, O. Y. 2005, *ApJ*, 623, 650

- Kruijssen, J. M. D., Pelupessy, F. I., Lamers, H. J. G. L. M., Portegies Zwart, S. F., & Icke, V. 2011, *MNRAS*, 414, 1339
Kruijssen, J. M. D., Pfeffer, J. L., Chevalance, M., et al. 2020, *MNRAS*, 498, 2472
Kruijssen, J. M. D., Pfeffer, J. L., Crain, R. A., & Bastian, N. 2019a, *MNRAS*, 486, 3134
Kruijssen, J. M. D., Pfeffer, J. L., Reina-Campos, M., Crain, R. A., & Bastian, N. 2019b, *MNRAS*, 486, 3180
Lahén, N., Naab, T., Johansson, P. H., et al. 2020, *ApJ*, 891, 2
Laporte, C. F. P., White, S. D. M., Naab, T., & Gao, L. 2013, *MNRAS*, 435, 901
Leaman, R., VandenBerg, D. A., & Mendel, J. T. 2013, *MNRAS*, 436, 122
Lee, Y. W., Joo, J. M., Sohn, Y. J., et al. 1999, *Nature*, 402, 55
Leon, S., Meylan, G., & Combes, F. 2000, *A&A*, 359, 907
Li, H., Gnedin, O. Y., Gnedin, N. Y., et al. 2017, *ApJ*, 834, 69
Li, H., Vogelsberger, M., Bryan, G. L., et al. 2022, *MNRAS*, 514, 265
Libeskind, N. I., Carlesi, E., Grand, R. J. J., et al. 2020, *MNRAS*, 498, 2968
Lux, H., Read, J. I., & Lake, G. 2010, *MNRAS*, 406, 2312
Ma, X., Grudić, M. Y., Quataert, E., et al. 2020, *MNRAS*, 493, 4315
Mackereth, J. T. & Bovy, J. 2020, *MNRAS*, 492, 3631
Mackey, A. D. & van den Bergh, S. 2005, *MNRAS*, 360, 631
Majewski, S. R., Patterson, R. J., Dinescu, D. I., et al. 2000, in *Liege International Astrophysical Colloquia*, Vol. 35, *Liege International Astrophysical Colloquia*, ed. A. Noels, P. Magain, D. Caro, E. Jehin, G. Parmentier, & A. A. Thoul, 619
Majewski, S. R., Schiavon, R. P., Frinchaboy, P. M., et al. 2017, *AJ*, 154, 94
Malhan, K., Ibata, R. A., Sharma, S., et al. 2022, *ApJ*, 926, 107
Massari, D., Dalessandro, E., Erkal, D., et al. 2024, *arXiv e-prints*, arXiv:2405.13498
Massari, D., Koppelman, H. H., & Helmi, A. 2019, *A&A*, 630, L4
McMillan, P. J. 2017, *MNRAS*, 465, 76
Meng, X. & Gnedin, O. Y. 2022, *MNRAS*, 515, 1065
Mori, A., Di Matteo, P., Salvadori, S., et al. 2024, *A&A*, 690, A136
Myeong, G. C., Evans, N. W., Belokurov, V., Sanders, J. L., & Koposov, S. E. 2018, *ApJ*, 863, L28
Navarro, J. F., Frenk, C. S., & White, S. D. M. 1997, *ApJ*, 490, 493
Nelson, D., Pillepich, A., Springel, V., et al. 2019a, *MNRAS*, 490, 3234
Nelson, D., Springel, V., Pillepich, A., et al. 2019b, *Computational Astrophysics and Cosmology*, 6, 2
Newton, O., Davies, J. J., Pfeffer, J., et al. 2024, *arXiv e-prints*, arXiv:2409.04516
Pagnini, G., Di Matteo, P., Haywood, M., et al. 2025a, *A&A*, 693, A155
Pagnini, G., Di Matteo, P., Haywood, M., et al. 2025b, *A&A*, 693, A155
Pagnini, G., Di Matteo, P., Khoperskov, S., et al. 2023, *A&A*, 673, A86
Park, S.-M., Shin, J., Smith, R., & Chun, K. 2022, *ApJ*, 941, 91
Petts, J. A., Read, J. I., & Gualandris, A. 2016, *MNRAS*, 463, 858
Pfeffer, J., Kruijssen, J. M. D., Crain, R. A., & Bastian, N. 2018, *MNRAS*, 475, 4309
Pfeffer, J., Lardo, C., Bastian, N., Saracino, S., & Kamann, S. 2021, *MNRAS*, 500, 2514
Pfeffer, J. L., Trujillo-Gomez, S., Kruijssen, J. M. D., et al. 2020, *MNRAS*, 499, 4863
Pillepich, A., Nelson, D., Springel, V., et al. 2019, *MNRAS*, 490, 3196
Pillepich, A., Sotillo-Ramos, D., Ramesh, R., et al. 2024, *MNRAS*, 535, 1721
Pillepich, A., Springel, V., Nelson, D., et al. 2018, *MNRAS*, 473, 4077
Ramos-Almendares, F., Sales, L. V., Abadi, M. G., et al. 2020, *MNRAS*, 493, 5357
Reina-Campos, M., Keller, B. W., Kruijssen, J. M. D., et al. 2022, *MNRAS*, 517, 3144
Renaud, F. 2020a, in *IAU Symposium*, Vol. 351, *Star Clusters: From the Milky Way to the Early Universe*, ed. A. Bragaglia, M. Davies, A. Sills, & E. Vesperini, 40–46
Renaud, F. 2020b, in *IAU Symposium*, Vol. 351, *Star Clusters: From the Milky Way to the Early Universe*, ed. A. Bragaglia, M. Davies, A. Sills, & E. Vesperini, 40–46
Renaud, F., Agertz, O., & Gieles, M. 2017a, *MNRAS*, 465, 3622
Renaud, F., Agertz, O., & Gieles, M. 2017b, *MNRAS*, 465, 3622
Rodriguez, C. L., Hafen, Z., Grudić, M. Y., et al. 2023, *MNRAS*, 521, 124
Saifollahi, T., Lançon, A., Cantiello, M., et al. 2025a, *arXiv e-prints*, arXiv:2503.16367
Saifollahi, T., Voggel, K., Lançon, A., et al. 2025b, *A&A*, 697, A10
Sameie, O., Boylan-Kolchin, M., Hopkins, P. F., et al. 2023, *MNRAS*, 522, 1800
Snaith, O., Haywood, M., Di Matteo, P., et al. 2015, *A&A*, 578, A87
Sotillo-Ramos, D., Pillepich, A., Donnari, M., et al. 2022, *MNRAS*, 516, 5404
Sun, G., Wang, Y., Liu, C., et al. 2023, *Research in Astronomy and Astrophysics*, 23, 015013
Tsuchiya, T., Dinescu, D. I., & Korchagin, V. I. 2003, *ApJ*, 589, L29
Tsuchiya, T., Korchagin, V. I., & Dinescu, D. I. 2004, *MNRAS*, 350, 1141
van den Bergh, S. 2012, *ApJ*, 746, 189
Vasiliev, E. 2019, *MNRAS*, 482, 1525
Vasiliev, E. & Baumgardt, H. 2021, *MNRAS*, 505, 5978
Weinberger, R., Springel, V., Hernquist, L., et al. 2017, *MNRAS*, 465, 3291

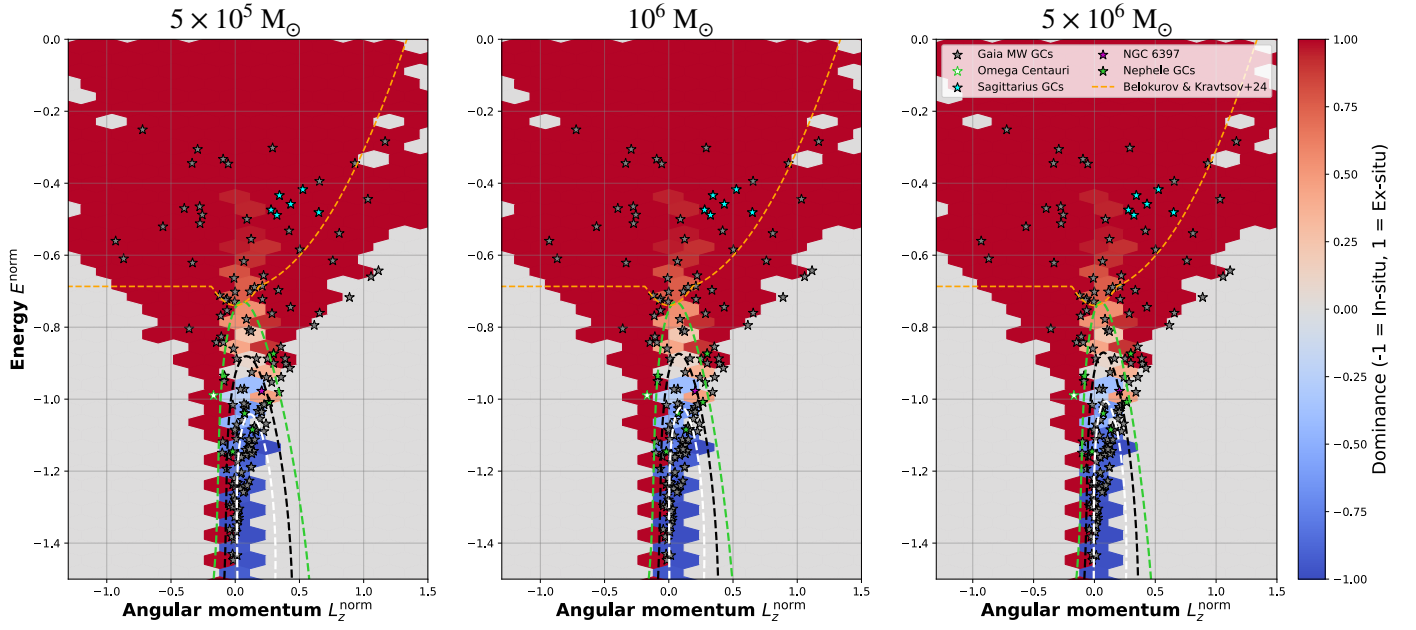


Fig. A.2. *Mass impact:* Normalized total energy as function of the normalized z-component of the angular momentum at $z = 0$ for both in-situ and ex-situ GCs for the 198 MWs in the full MW potential + dynamical friction. The decision boundaries in dashed lines corresponding to probabilities of 0.05 (magenta), 0.5 (black), and 0.95 (green) are plotted to illustrate the separation between the two populations. It was found that our results remain unchanged within a reasonable initial mass range for globular clusters ($0.5 - 5 \times 10^6 M_\odot$).